Green and Scalable Synthesis of a Dual-ligand Zn-MOF with Unprecedented Space-time Yield in Aqueous Media and Efficient CH_4/N_2 Separation

*Zhang-Ye Han[1], Xuefeng Bai[1], Yan-Long Zhao[1], Wen-Liang Li[1], Quanyou Sun[1], Zheng-He Xie[2], Li-Feng Ding[2], Rui Li[*1], and Jian-Rong Li[*1]*

1. Beijing Key Laboratory for Green Catalysis and Separation and Department of Chemical Engineering, College of Materials Science and Engineering, Beijing University of Technology, Beijing, P. R. China 100124.

2. Beijing Energy Holding Co., Ltd., Beijing, People's Republic of China 100022.

* Corresponding authors.

E-mail addresses: jrli@bjut.edu.cn (J.-R. Li), lirui1@bjut.edu.cn (R. Li).

Experimental Methods

1. Material

Zinc chloride, zinc sulfate, and sodium acetate were purchased from Shanghai Macklin Biochemical Co., Ltd. Zinc acetate dihydrate and isophthalic acid were purchased from Shanghai Bide Pharmaceutical Technology Co. Zinc nitrate hexahydrate and sodium hydroxide were purchased from Beijing Yili Fine Chemicals Co, Ltd. and Meryer (Shanghai) Chemical Technology Co., Ltd., respectively. 3-Amino-1,2,4-Triazole was purchased from Tianjin Xiensi Biochemical Technology Co. All chemicals were used as received without any further purification. Deionized (DI)

water used in all experiments was purified with a Siemens Ultra Clear TWF water purification system.

2. Synthesis procedure

2.1 Traditional solvothermal synthesis route

A previously reported synthesis protocol was adopted.[1] Typically, a mixture of $Zn(NO_3)_2 \cdot 6H_2O$ (1.0 mmol, 0.298 g), isophthalic acid (0.5 mmol, 0.083 g), 3-amino-1,2,4-triazole (1.0 mmol, 0.084 g), DMF (4 mL), MeOH (4 mL), and H_2O (2 mL) was sealed in a 15 mL stainless steel reactor at 130℃ for 72 h. After decanting the mother liquor, the colorless crystalline product was rinsed three times with fresh DMF and MeOH, then dried in air for 12 h (yield ~78% based on Zn).

2.2 Optimization of the anions

NaOH (0.160 g, 4 mmol) and isophthalic acid (0.332 g, 2 mmol) were mixed in 30 mL water to form sodium isophthalate (Na_2ipa). Then 3-amino-1,2,4-triazole (0.336 g, 4 mmol), $Zn(NO_3)_2 \cdot 6H_2O$ (1.192 g, 4 mmol), and different amounts of NaOAc (0 mg, 0.041 mg, 0.164 mg, 0.656 g, 0.984 mg) were successively added into the mixture, resulting in the immediate formation of a white precipitate. The mixture was stirred for 2 h under ambient conditions. Then the obtained solid was filtered, washed with water and dried at 120°C for 12 h. The syntheses using other metal salts employed the same procedure, with the exception of zinc acetate.

For the MOF synthesized using $Zn(OAc)_2 \cdot 2H_2O$ as the metal source, NaOH (0.160 g, 4 mmol) and isophthalic acid (0.332 g, 2 mmol) were first mixed in 30 mL water to form Na_2ipa. Then 3-amino-1,2,4-triazole (0.336 g, 4 mmol) and $Zn(OAc)_2 \cdot 2H_2O$ (0.876 g, 4 mmol) were successively added into the mixture, which was stirred for an additional 2 h. The white product was obtained by filtering and washing, followed by drying overnight in 120°C. (≈83% yield).

2.3 Optimization of the addition sequence of ingredients

Scenario (1): $Zn(OAc)_2 \cdot 2H_2O$ (0.876 g, 4 mmol) and 3-amino-1,2,4-triazole (0.336 g, 4 mmol) were mixed in 20 mL water, resulting in the immediate formation of a white precipitate. After 5 min of stirring, a 10 mL solution of Na_2ipa (2 mmol) was

added, followed by room temperature synthesis for specific durations with continuous stirring. The obtained solid was filtered, washed and dried at 120°C for 12 h.

Scenario (2): Na_2ipa (2 mmol) and 3-amino-1,2,4-triazole (0.336 g, 4 mmol) were combined in 20 mL water. After 5 min stirring, a 10 mL solution of $Zn(OAc)_2 \cdot 2H_2O$ (0.876 g, 4 mmol) was introduced. Room temperature synthesis for specific durations was conducted with continuous stirring, and the obtained solid was filtered, washed with water, and dried at 120°C for 12 h.

Scenario (3): Na_2ipa (2 mmol) and $Zn(OAc)_2 \cdot 2H_2O$ (0.876 g, 4 mmol) were combined in 20 mL water. After 5 min stirring, a 10 mL solution of 3-amino-1,2,4-triazole (0.336 g, 4 mmol) was introduced. The mixture was stirred at room temperature for specific durations to obtain the solid product, which was filtered, washed with water, and dried at 120°C for 12 h.

2.4 Optimization of the concentrations.

The optimal synthesis condition was determined by systematically changing the concentrations of $Zn(OAc)_2 \cdot 2H_2O$, 3-amino-1,2,4-triazole, and ipa^{2-} with a constant molar ratio of ingredients and a maintained volume of solvent. Under the optimal condition, 5.35 mL Na_2ipa (1.88 mol/L, 10 mmol) and 7.5 mL 3-amino-1,2,4-triazole (2.67 mol/L, 20 mmol) were mixed into a 100 mL round bottomed flask. Next, 12.75 mL $Zn(OAc)_2 \cdot 2H_2O$ (1.57 mol/L, 20 mmol) was added, and the mixture was stirred at ambient temperature for 2 h. After filtering, the obtained solid was washed with water, and dried at 120°C for 12 h. (≈83% yield)

2.5 Optimization of the ratio of H_2ipa: NaOH

Firstly, H_2ipa (1.66 g, 10 mmol) was mixed with different amounts of NaOH (0.8 g, 1.2 g, 1.6 g, 2 g) in 5 mL water. Then 7.5 mL 3-amino-1,2,4-triazole (2.67 mol/L, 20 mmol) and 12.75 mL $Zn(OAc)_2 \cdot 2H_2O$ (1.57 mol/L, 20 mmol) were successively added. The reaction mixture was stirred at room temperature for 2 h, the obtained solid was filtered, washed with water, and dried at 120°C for 12 h.

2.6 Optimization of synthesis temperature and time

5.3 mL Na_2ipa (1.88 mol/L, 10 mmol), 7.5 mL 3-amino-1,2,4-triazole (2.67 mol/L,

20 mmol) and 12.75 mL $Zn(OAc)_2 \cdot 2H_2O$ (1.57 mol/L, 20 mmol) were successively mixed in a round-bottom flask. The reaction mixture was heated under 20℃, 40℃, 60℃, 80℃ for 2 h. After filtration, washing with water and drying at 120℃ for 12 h, a white powder of $Zn_2(atz)_2ipa$ was obtained.

2.7 Kilogram-scale synthesis of $Zn_2(atz)_2ipa$

Scale-up synthesis was carried out in a 10 L reactor with a circulating oil bath to maintain the temperature at 60℃. The amounts of ingredients were increased by 275 times. First, 1.2 L Na_2ipa solution (1.88 mol/L, 2.25 mol) was mixed with 2.1 L 3-amino-1,2,4-triazole solution (2.67 mol/L, 5.5 mol). Subsequently, 3.5 L $Zn(OAc)_2 \cdot 2H_2O$ solution (1.57 mol/L, 5.5 mol) was added under stirring. After heated at 60℃ for varied periods of time, the product was timely filtered and washed with 20 L water for 3 times. After drying at 120℃ for 12 h, a white powder was obtained (1.16 kg, ≈91.3% yield, based on the Zn).

3. Calculation of space-time yield (STY)

The STY is one of the key parameters assessing the viability of the manufacturing method, which can be calculated as：

$$\mathrm{STY} = \frac{M_p}{V_e \cdot T} \quad (Eq\ 1)$$

where M_p is mass of product (kg), V_e is the effective volume of the reactor (m^3), T is the reaction time (day).

4. Water stability tests

A certain amount of the product (5 g) is placed in a sealed flask with excessive water. After 1 month, the product is recovered by filtration and drying to characterize the mass and physicochemical properties (PXRD, TGA, BET adsorption). The stability of the product is thus evaluated.

5. Powder X-ray diffraction (PXRD)

PXRD was conducted to verify the structure and phase purity of $Zn_2(atz)_2ipa$. The data was collected with a Rigaku SmartLab3 diffractometer (Cu Kα radiation, λ = 1.542 Å) from 5° to 30° (2θ range) at a step of 5 ~ 10° per minute. The sample powders were spread on glass substrates for the tests. The simulated XRD pattern was generated from

the crystal structure (i.e., the cif file).

6. Thermogravimetry analysis (TGA)

To confirm the thermal stability of $Zn_2(atz)_2ipa$, TGA was carried out on the LABSYS EVO equipment. The sample was heated from ambient temperature to 800°C under N_2 atmosphere at a heating rate of 10 °C/min.

7. Brunaue-Emmett-Teller (BET) surface areas

The BET surface areas of samples were evaluated from the N_2 adsorption isotherms at 77 K using *Eq 2* below.

$$S_{BET} = \frac{N_A \partial}{22414\,(K + I)} \quad (Eq\ 2)$$

where N_A is Avogadro's constant, ∂ is the cross-sectional area of each adsorbent molecule, and 22414 is the volume (mL) of 1 mole ideal gas at the standard temperature and pressure. K and I represent the slope and intercept of the fitted line, respectively.

Take $Zn_2(atz)_2ipa$-(*kg*) as an example：

$S_{BET} = 6.023\times10^{23}\times0.162\times10^{-18}/(22414\times(0.00633+1.16585\times10^{-6})) = 687.6\ m^2/g$

8. Calculation of isosteric heat of adsorption

The bonding energy between the adsorbate molecules and the adsorbent lattice atoms is reflected in the isosteric heat of adsorption $(Q_{st})^2$, which is defined as:

$$Q_{\mathrm{st}} = R\sum_{i=0}^{m} a_i N^i \ (Eq\ 3)$$

$$\ln P = \ln N + \frac{1}{T}\sum_{i=0}^{m} a_i N^i + \sum_{j=0}^{m} b_j N^j \ (Eq\ 4)$$

where Q_{st} is the coverage-dependent enthalpy of adsorption, R is the universal gas constant, P represents the pressure (mmHg), T represents the temperature (K), N is the adsorbed amount (mg/g), a_i and b_j are Virial coefficients and m, n represent the numbers of coefficients used to adequately describe the adsorption curves. The values of a_0 through a_m were used to calculate the isosteric heat of adsorption using *Eq 3*.

9. Fitting of single-component adsorption isotherms

The experimentally measured CH_4 and N_2 loadings of samples at 298 K were fitted with the 1-site, 2-site, or 3-site-Langmuir isotherm model:

1-site-Langmuir isotherm model: $N = A \times \frac{bP^C}{1+bP^C}$ (*Eq* 5)

2-site-Langmuir isotherm model: $N = A \times \frac{b_1P^{C_1}}{1+b_1P^{C_1}} + A_2 \times \frac{b_2P^{C_2}}{1+b_2P^{C_2}}$ (*Eq* 6)

3-site-Langmuir isotherm model: $N = A \times \frac{b_1P^{C_1}}{1+b_1P^{C_1}} + A_2 \times \frac{b_2P^{C_2}}{1+b_2P^{C_2}} + A_3 \times \frac{b_3P^{C_3}}{1+b_3P^{C_3}}$ (*Eq* 7)

where *N* is the adsorbed amount per gram of adsorbent (mmol/g), *P* is the pressure of the bulk gas at equilibrium with the adsorbed phase (kPa), A is the saturation capacities of sites A (mmol/g), b is the affinity coefficients of sites A (1/kPa), and C represents the deviations from an ideal homogeneous surface. The fitting parameters of *Eqs 5-7* are listed in the lower right tables of Figure S18.

10. Ideal adsorbed solution theory (IAST)

IAST calculations were performed to evaluate the CH_4/N_2 separation performance. The adsorption selectivity of component 1 (CH_4) over component 2 (N_2) in a binary mixture can be defined by:

$$S_{1,2} = \frac{q_1/q_2}{y_1/y_2} \quad (Eq\ 8)$$

In *Eq 8*, the q_1 and q_2 represent the equilibrated molar loadings of CH_4 and N_2, expressed in mol/kg^{-1}; y_1, and $y_2 = 1 - y_1$, represent the mole fractions of CH_4 and N_2 in the bulk gas phase. As an example, the IAST calculations of a 50/50 mixture at 298 K adopted the mole fractions of $y_1 = 0.5$ and $y_2 = 1 - y_1 = 0.5$ for a range of pressures up to 110 kPa.

11. Computational Details.

DFT calculations were carried out using the CP2K code.[3] All calculations employed mixed Gaussian and planewave basis sets. Core electrons were represented with norm-conserving Goedecker-Teter-Hutter pseudopotentials,[4-6] and the valence electron wavefunction was expanded in a double-zeta basis set with polarization functions[7] along with an auxiliary plane wave basis set with an energy cutoff of 360 Ry.

The generalized gradient approximation exchange-correlation functional of Perdew, Burke, and Enzerhof (PBE)[8] was used. Each configuration was optimized with the OT algorithm with SCF convergence criteria of 1.0×10^{-8} au. To compensate for the long-range van der Waals dispersion interaction between the adsorbate and the MOFs, the DFT-D3 scheme[9] with an empirical damped potential term was added into the energies obtained from exchange-correlation functional in all calculations.

The adsorption energy between the adsorbate and the $Zn_2(atz)_2ipa$ can be calculated using the following equation:

$$\Delta E_{ads}=E_{adsorbate@MOF}-E_{MOF}-E_{adsorbate} \quad (Eq\ 9)$$

In *Eq 9*, $E_{adsorbate@MOF}$ and E_{MOF} represent the total energies of the substrate with and without adsorbate, respectively. $E_{adsorbate}$ is the energy of the adsorbate. According to this equation, a negative adsorption energy suggests a stable adsorption configuration.

12. Breakthrough experiments

To verify the ability of $Zn_2(atz)_2ipa$ to separate the CH_4/N_2 mixture under dynamic conditions, breakthrough experiments were performed at 298 K and 1 bar. The sample powder (about 2.8 g) was filled into a cylindrical stainless steel breakthrough column (4.5 × 210 mm) and was degassed at 393 K under a dynamic vacuum for 12 h to remove solvent molecules before the experiments. The flow rate and the pressure at the inlet are controlled by a mass flow controller and a pressure sensor, respectively. The CH_4/N_2 (50/50, 30/70, and 15/85, v/v) mixtures were fed into the breakthrough column at a flow rate of 3.0 mL/min. The effluent gas was detected by a gas chromatograph.

Tables

Table S1. Effects of sodium acetate quantity and the metal sources

No.	Metal source (mmol)	atz (mmol)	H_2ipa (mmol)	NaOH (mmol)	NaOAc (mmol)	Time (h)	Yield (%)	BET (cm^3/g)
1	$Zn(NO_3)_2·6H_2O$ (4)	4	2	4	0	2	—	—
2	$Zn(NO_3)_2·6H_2O$ (4)	4	2	4	0.5	2	36%	646
3	$Zn(NO_3)_2·6H_2O$ (4)	4	2	4	2	2	64%	690
4	$Zn(NO_3)_2·6H_2O$ (4)	4	2	4	8	2	82%	680
5	$Zn(NO_3)_2·6H_2O$ (4)	4	2	4	12	2	81%	679
6	$ZnSO_4$ (4)	4	2	4	0	2	—	—
7	$ZnSO_4$ (4)	4	2	4	8	2	78%	640
8	$ZnCl_2$ (4)	4	2	4	0	2	—	—
9	$ZnCl_2$ (4)	4	2	4	8	2	80%	718
10	$Zn(OAc)_2$ (4)	4	2	4	0	2	83%	710

Table S2. Effects of the reagent concentrations

No.	$Zn(OAc)_2·2H_2O$ (mmol)	atz (mmol)	H_2ipa (mmol)	NaOH (mmol)	V_{total} (mL)	Time (h)	Yield (%)	BET (cm^3/g)
1	5	5	2.5	5	25.6	2	82%	694
2	10	10	5	10	25.6	2	85%	725
3	15	15	7.5	15	25.6	2	81%	709
4	20	20	10	20	25.6	2	83%	711

Table S3. Effects of the H_2ipa: NaOH ratio

No.	$Zn(OAc)_2·2H_2O$ (mmol)	atz (mmol)	H_2ipa (mmol)	NaOH (mmol)	V_{total} (mL)	Time (h)	Yield (%)	BET (cm^3/g)
1	20	20	10	20	25.6	2	83%	677
2	20	20	10	30	25.6	2	85%	685
3	20	20	10	40	25.6	2	81%	379
4	20	20	10	50	25.6	2	0	—

Table S4. Effects of the synthesis temperature

No.	$Zn(OAc)_2·2H_2O$ (mmol)	atz (mmol)	H_2ipa (mmol)	NaOH (mmol)	V_{total} (mL)	Temp. (℃)	Yield (%)	BET (cm^3/g)
1	20	20	10	20	25.6	20	83%	677
2	20	20	10	20	25.6	40	81%	680
3	20	20	10	20	25.6	60	91%	736
4	20	20	10	20	25.6	80	89%	647

Table S5. CH_4/N_2 separation performances of representative porous adsorbents at 298 K, taking from the previous literature. The performance of $Zn_2(atz)_2ipa$-(*kg*) was shown as a comparison.

Adsorbent	CH_4/N_2 selectivity	CH_4 uptake (cm^3/g)	N_2 uptake (cm^3/g)	Q_{st} of CH_4 (kJ/mol)	Ref.
$Ni(INA)_2$	15.8	46.7	14.5	28.0	10
Al-CDC	13.1	32.0	5.1	27.5	11
$Co_3(C_4O_4)_2(OH)_2$	12.5	19.8	9.1	25.1	12
CAU-21-BPDC	11.9	22.2	4.2	20.5	13
CoNi(pyz-NH_2)	11.9	20.0	3.0	25.5	14
SBMOF-1	11.5	20.6	4.0	23.5	15
ATC-Cu	9.7	64.9	16.8	26.8	16
NKMOF-8-Me	9.0	39.5	7.0	28.0	17
Al-FUM-Me	8.6	27.3	5.0	24.1	18
MOF-888	8.4	10.0	1.8	26.0	19
$Cu(INA)_2$	8.3	18.6	2.7	17.5	20
MOF-891	7.8	30.0	6.4	22.0	19
ZIF-94	7.4	33.6	8.2	23.9	21
Ni-Qc-5-Dia	7.4	29.3	6.2	19.5	22
Ni-MA-BPY	7.4	22.6	4.7	23.5	23
Co-MA-BPY	7.2	20.6	4.3	18.4	23
DMOF-A2	7.2	37.0	8.8	22.5	24
CAU-10	7.2	16.6	5.3	7.1	25
TUTJ-201Ni	7.2	19.8	5.0	24.5	26
$Ni(OAc)_2L$	7.0	25.7	10.5	26.7	27
MOF-890	7.0	24.0	6.0	23.0	19
$Cu(hfipbb)(H_2hfipbb)_{0.5}$	6.9	10.5	2.9	24.0	28
MOF-889	6.4	26.0	5.3	22.0	19
TUT-100	6.3	27.5	5.0	23.7	29
$[Ni_3(HCOO)_6]$	6.2	18.4	4.0	—	30
MIL-120Al	6.0	33.7	10.5	20.9	31
$[Co_3(HCOO)_6]$	5.1	11.0	2.7	23.0	32
UiO-66-Br_2	5.1	16.1	4.4	—	33
UTSA-30a	5.0	14.1	3.69	—	34
$Cu(OTf)_2$	4.8	5.7	1.6	19.6	35
PAF-26-COOH	4.2	12.1	3.0	14.0	36
[Cu(Me-4py-trz-ia)]	4.2	25.1	—	18.0	37
MOF-177	4.0	12.5	3.0	11.7	38
MIL-53(Al)	3.7	16.6	5.0	19.0	37
Cu-BTC	3.7	20.0	7.8	—	39
Al-BDC	3.6	16.4	5.0	18.7	20
ZIF-93	3.6	11.7	3.6	15.8	21
ZIF-68	3.5	9.0	2.7	—	40
ZIF-69	3.0	11.2	3.1	—	40

Table S5. Continued

Adsorbent	CH_4/N_2 selectivity	CH_4 uptake (cm^3/g)	N_2 uptake (cm^3/g)	Q_{st} of CH_4 (kJ/mol)	Ref.
MIL-100(Cr)	3.0	13.5	3.8	—	41
ZIF-8	2.5	7.8	2.0	17.0	42
ZIF-90	2.3	10.6	4.5	15.9	21
ZK-5	4.3	18.3	7.5	—	43
Ca-SAPO-34	3.5	13.7	6.3	—	44
Na-SAPO-34	2.4~3.0	13.4	6.3	12.0	44
Zeolite 13X	1.9	10.3	2.8	14.7	45
Zeolite 5A	0.9	22.4	25.8	15	38
$Zn_2(atz)_2ipa$	6.2	18.2	4.5	28.0	**This work**

Table S6. Comparison of economic and environmental factors between $Zn_2(atz)_2ipa$ and other top-performing MOFs.

Adsorbents	Ligand	Ligand price (per kg)[a]	Synthesis solvent	Synthesis condition
$Ni(INA)_2$	isonicotinic acid	$30	acetonitrile/DMF	423 K, 72 h
Al-CDC	trans-1,4-Cyclohexanedicarboxylic acid	$103	DMF/H_2O	403 K, 5 min
$Co_3(C_4O_4)_2(OH)_2$	squaric acid	$1590	H_2O	493 K, 48 h
CAU-21-BPDC	4,4-carbonyldibenzoic acid	$8944	DMF/H_2O	383 K, 6 h
CoNi(pyz-NH_2)	$K_2[Ni(CN)_4]\cdot nH_2O$ 2-pyrazinyl amine	$5134 $207	H_2O/methanol	298 K, 3 h
SBMOF-1	4, 4-sulfonyldibenzoic acid	$8143	ethanol	453 K, 4 day
ATC-Cu	1, 3, 5, 7-adamantanetetracarboxylic	$230227	H_2O	463 K, 24 h
NKMOF-8-Me	2-methylimidazole-4, 5-dicarbonitrile	$126984	acetonitrile	298 K,1 min
Al-FUM-Me	Methylfumaric acid	$19296	DMF	403 K,4 day
$Zn_2(atz)_2ipa$ (**This work**)	3-amino-1,2,4-triazole isophthalic acid	$50 $8	H_2O	333 K, 10 min

a. Price data was queried from the official website of HEOWNS and Shanghai Bide Pharmaceutical Technology (www.heowns.com, www.bidepharm.com). An exchange rate from Chinese Yuan (CNY) to US Dollar (USD) of 7.26 was adopted in the calculation.

Table S7. Production cost of $Zn_2(atz)_2ipa$-(*kg*) compared with the market prices of selected molecular sieves.

Adsorbents	Price (per kg)[a]
$Zn_2(atz)_2ipa$	$32
ZSM-5	$110
SSZ-13	$220
SAPO-34	$166
SBA-15	$1102
MCM-41	$551

a. The selling prices of the molecular sieves were acquired from large manufacturers of Ze'er Catalytic (www.zrcat.com) and Jianlong (www.jalon.cn). An exchange rate from Chinese Yuan (CNY) to US Dollar (USD) of 7.26 was adopted in the calculation.

Figures

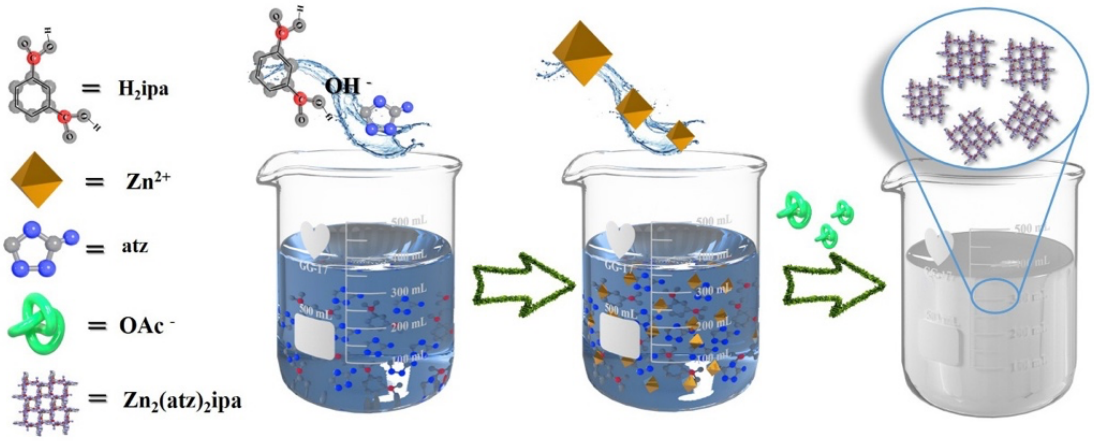

Figure S1. Scheme of the modulator/base co-regulated synthesis of $Zn_2(atz)_2ipa$.

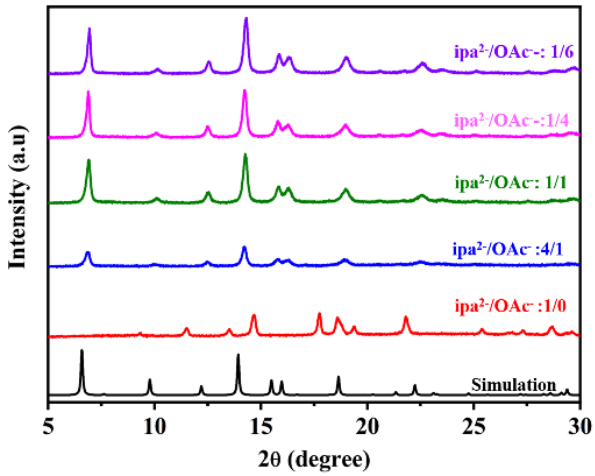

Figure S2. PXRD patterns of $Zn_2(atz)_2ipa$ prepared with different amounts of OAc^-.

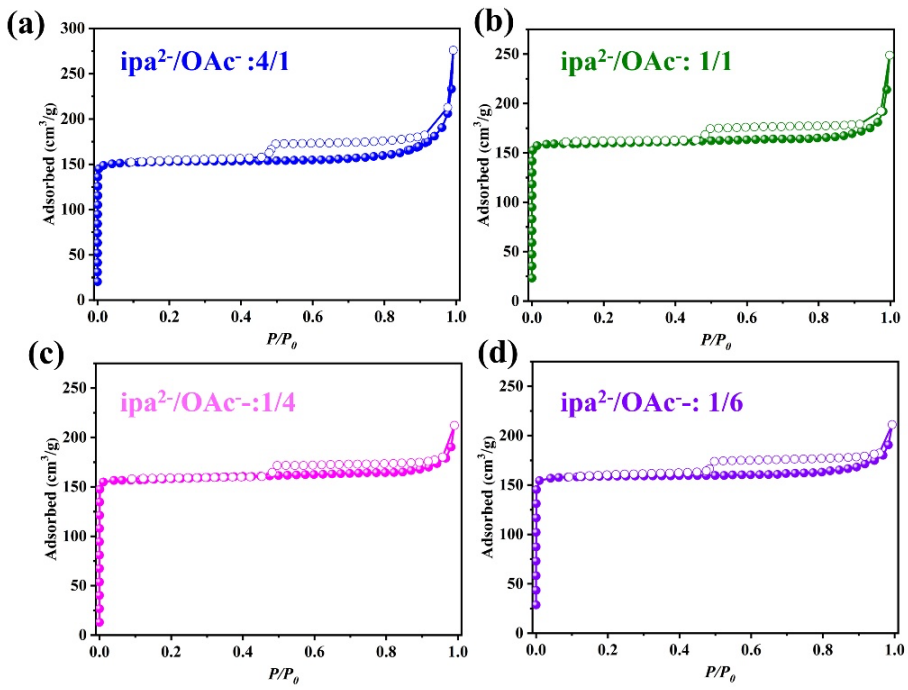

Figure S3. N_2 adsorption isotherms of $Zn_2(atz)_2ipa$ prepared with different amounts of OAc^- measured at 77 K.

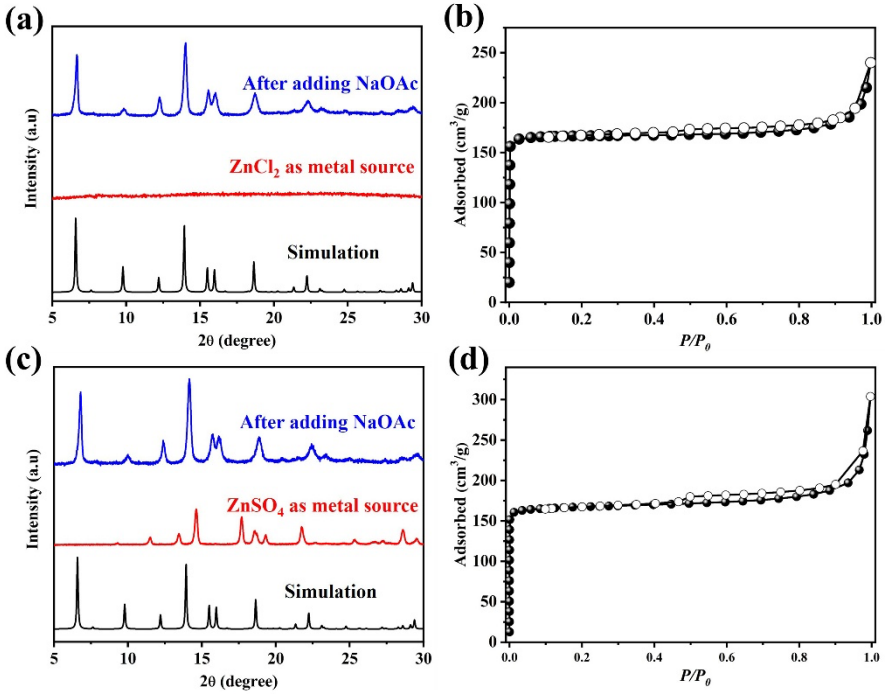

Figure S4. Effects of metal salts with altered anions. (a) PXRD patterns and (b) N_2 adsorption isotherms of samples prepared using $ZnCl_2$ without and with the addition of NaOAc. (c) PXRD patterns and (d) N_2 adsorption isotherms of samples prepared using $ZnSO_4$ without and with the addition of NaOAc. $Zn_2(atz)_2ipa$ is attainable only with the presence of OAc^-. All N_2 adsorption isotherms were measured at 77 K.

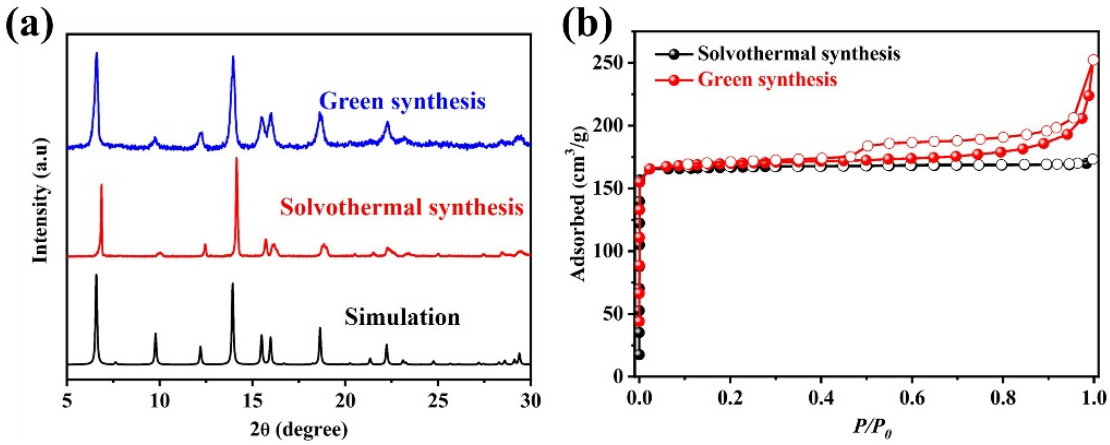

Figure S5. (a) PXRD patterns and (b) N_2 adsorption isotherms of $Zn_2(atz)_2ipa$ prepared using $Zn(OAc)_2$. Water was selected as the solvent and NaOAc was omitted. The $Zn_2(atz)_2ipa$ sample synthesized using the traditional solvothermal protocol was also characterized as a comparison.

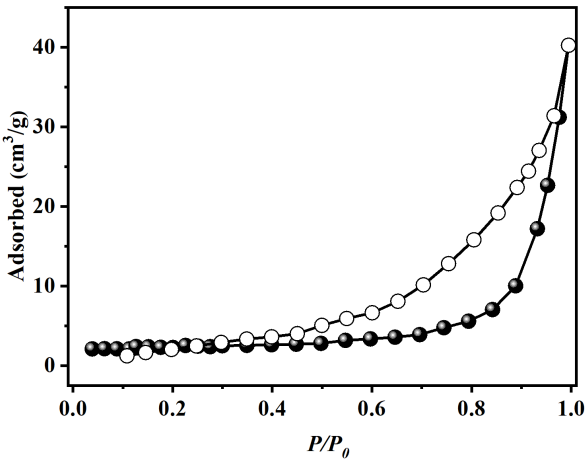

Figure S6. N_2 adsorption isotherm of the Zn-atz-OAc precursor. The low N_2 uptake attests the close-packed structure of the material**.**

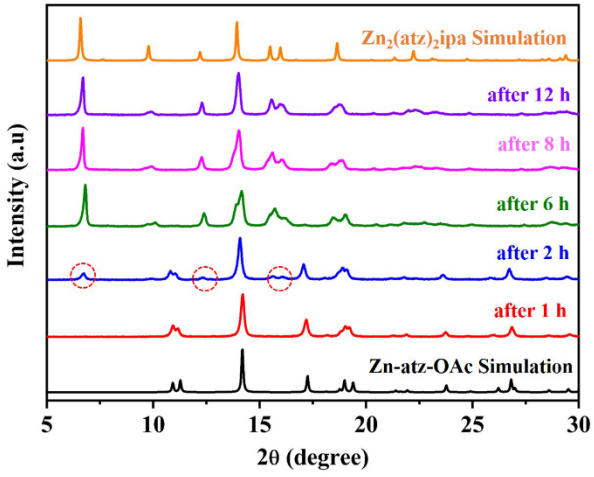

Figure S7. Temporal evolution of the PXRD patterns of the white solid prepared following scenario (1).

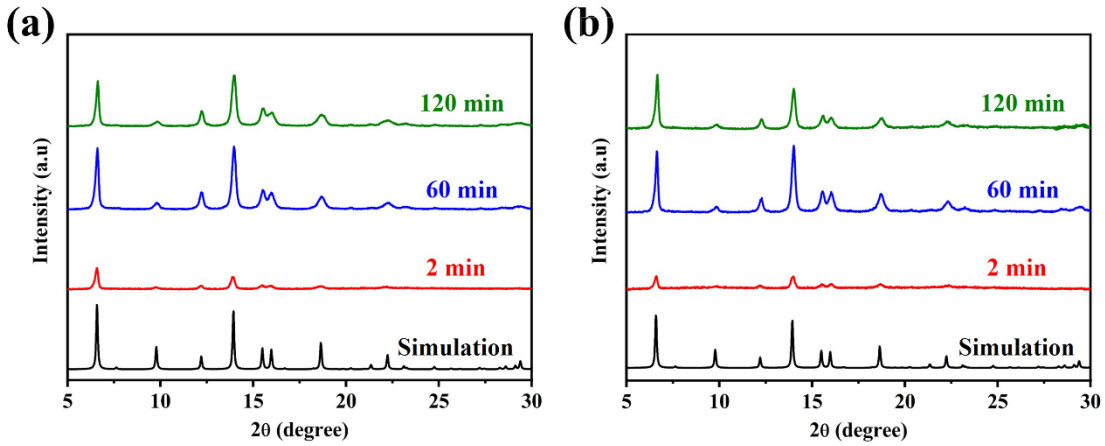

Figure S8. Temporal evolution of the PXRD patterns of $Zn_2(at)_2ipa$ prepared following (a) scenario (2) and (b) scenario (3).

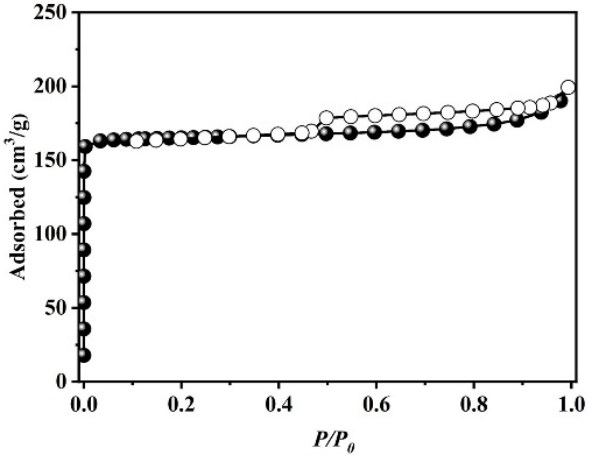

Figure S9. N_2 adsorption isotherms of the highly crystalline $Zn_2(at)_2ipa$ prepared following scenario (3) after 120 min synthesis.

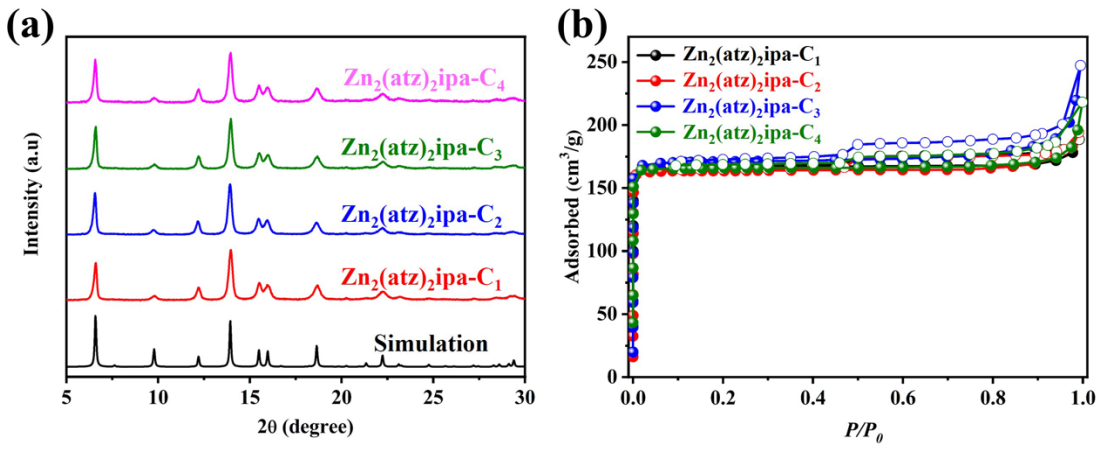

Figure S10. (a) PXRD patterns and (b) N_2 adsorption isotherms of $Zn_2(atz)_2ipa$ synthesized with altered solution concentrations. The C1-C4 samples correspond to the entries 1-4 in Table S2.

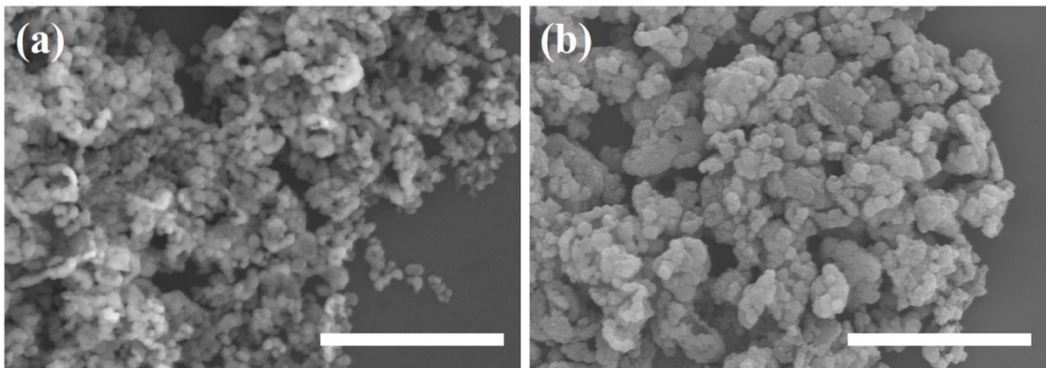

Figure S11. Electron micrographs of $Zn_2(atz)_2ipa$-C1 (a) and C4 (b) samples synthesized with altered solution concentrations. Similar crystal morphology and slightly larger particle size were observed for the $Zn_2(atz)_2ipa$ synthesized with higher solution concentration. The C1 and C4 samples correspond to the entries 1 and 4 in Table S2. Scale bars equal 10 μm.

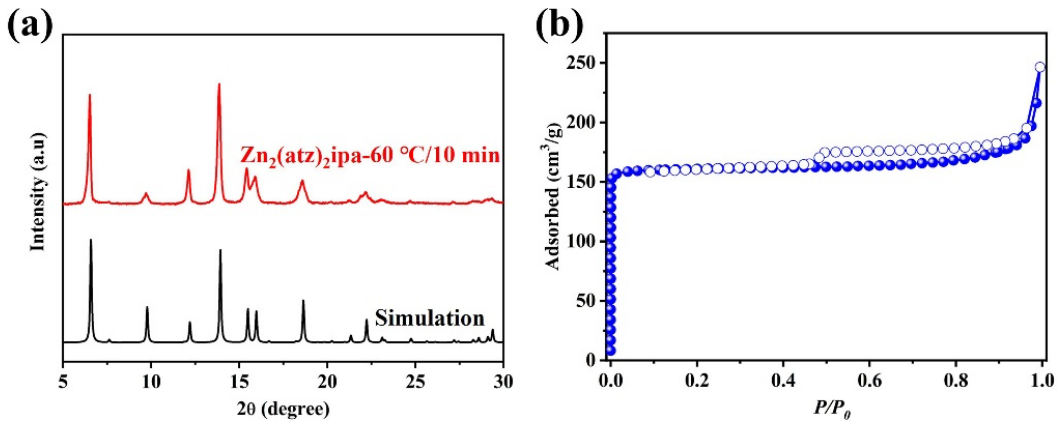

Figure S12. (a) PXRD pattern and (b) N_2 adsorption isotherm of $Zn_2(at)_2ipa$-60℃ with a heating time of 10 min.

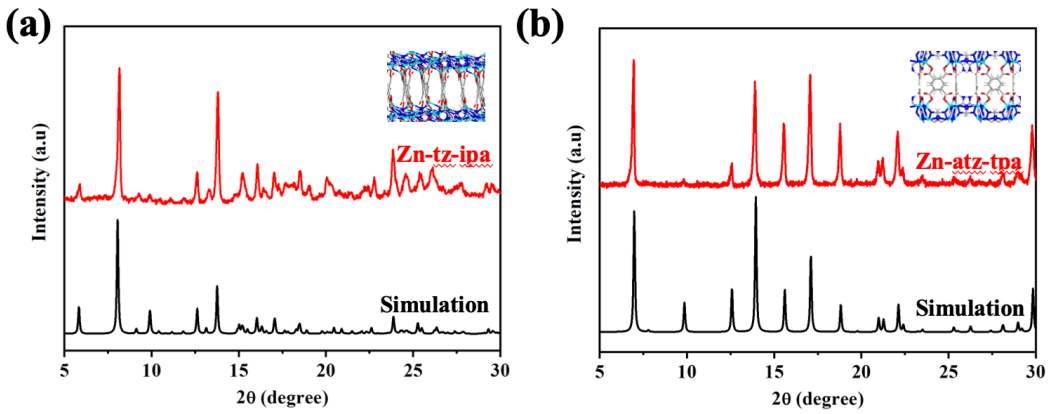

Figure S13. Diverse MOF structures synthesized in aqueous media using the reported co-regulation strategy. Variations were introduced to the molecular structures of the ligands to illustrate the broad applicability of the synthesis strategy: (a) 1,2,4-triazole (tz) was used instead of 3-amino-1,2,4-triazole (atz); (b) isophthalic acid (ipa) was replaced by terephthalic acid (tpa). The corresponding crystal structures of the products (CCDC 668599 and 917346, respectively) are demonstrated in each panel as insets.

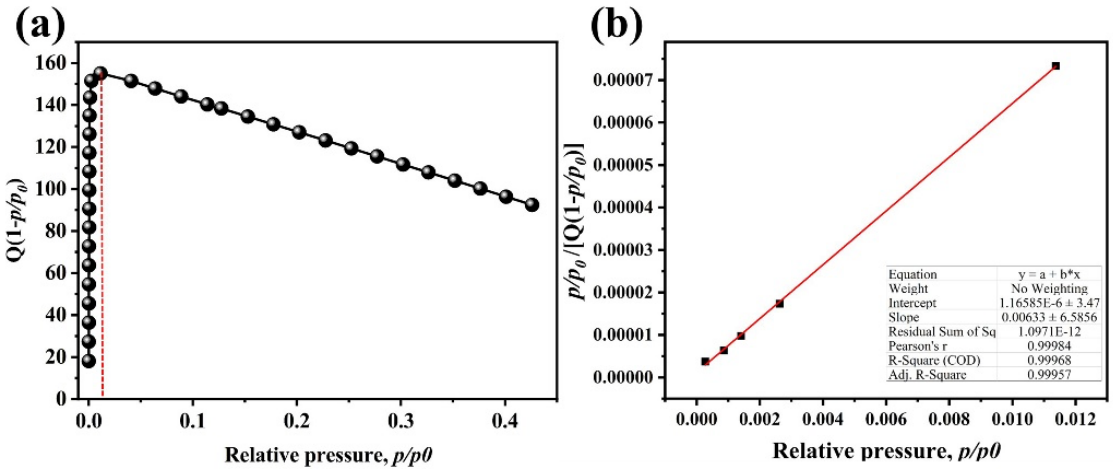

Figure S14. (a) The consistency plot and (b) the calculation of BET surface area for $Zn_2(atz)_2ipa$-(*kg*) based on its N_2 adsorption isotherm measured at 77 K.

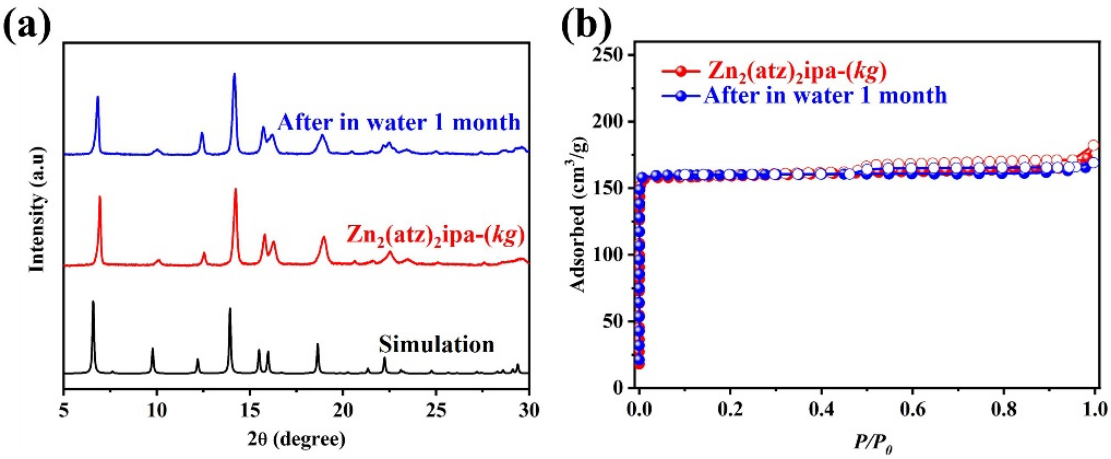

Figure S15. (a) PXRD patterns and (b) N_2 adsorption isotherms of $Zn_2(atz)_2ipa$-(*kg*) before and after one month of water exposure, indicating its remarkable stability.

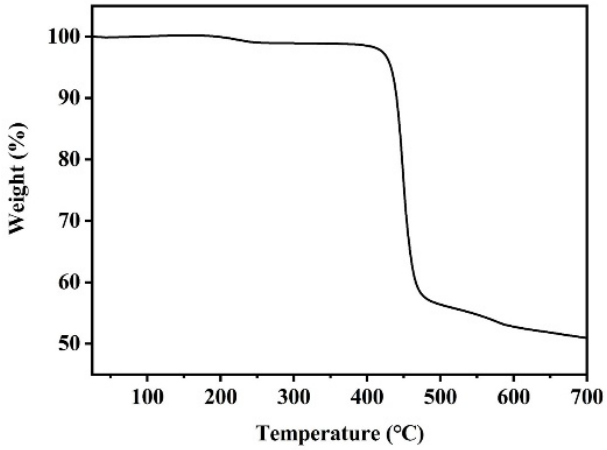

Figure S16. Thermogravimetric analysis (TGA) of $Zn_2(atz)_2ipa$-(*kg*), revealing its temperature tolerance exceeding 400°C.

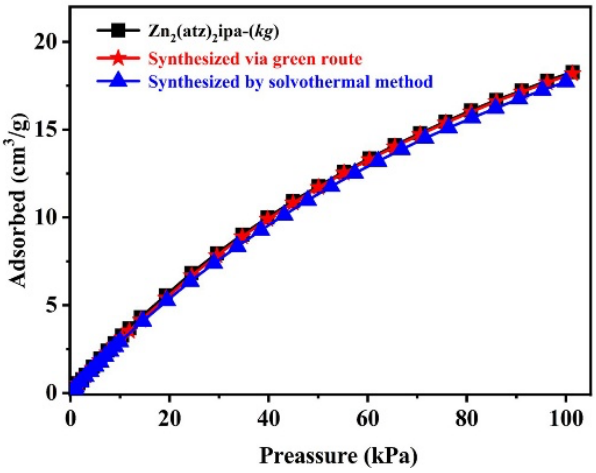

Figure S17. Comparison of CH_4 adsorption isotherms of the gram-scale (red), kilogram-scale (black), and solvothermally synthesized $Zn_2(atz)_2ipa$ (blue).

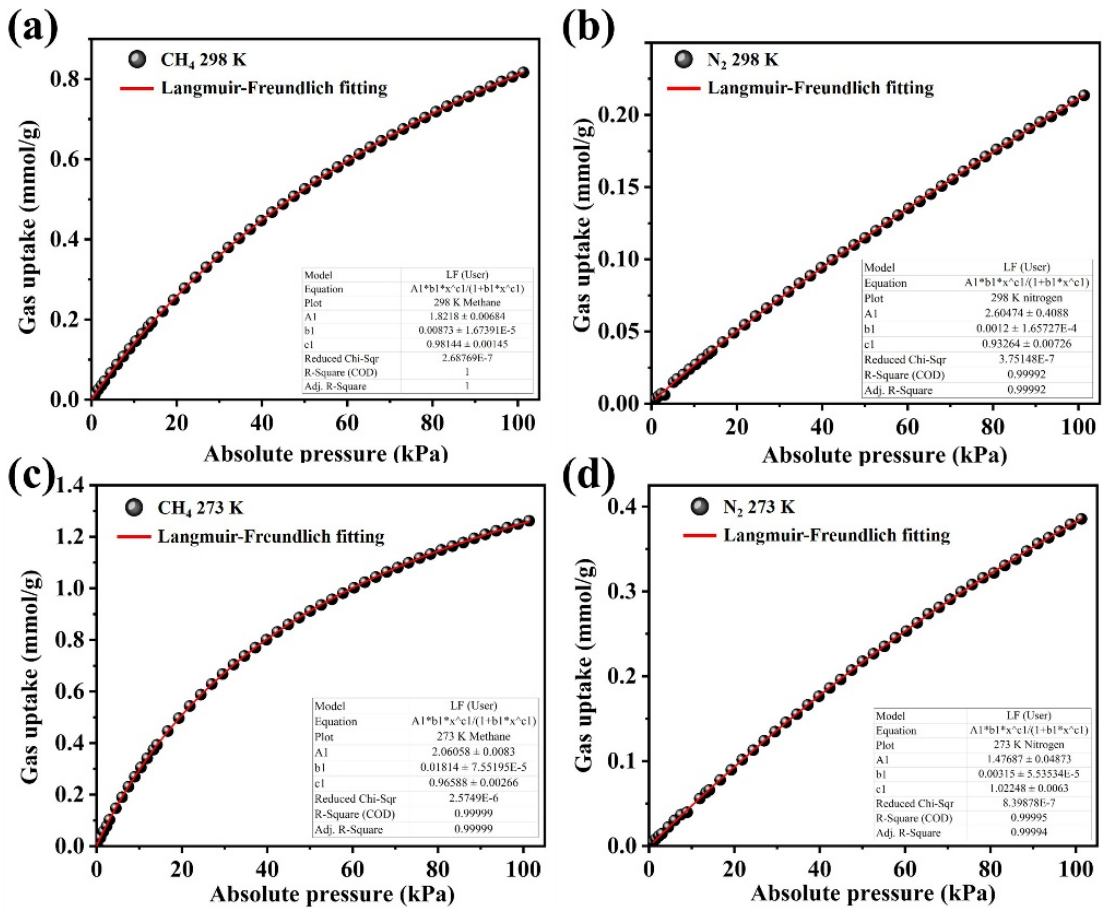

Figure S18. Langmuir-Freundlich fitting (red lines) of the adsorption isotherms (black points) of $Zn_2(atz)_2ipa$-(*kg*). (a) CH_4 and (b) N_2 at 298 K. (c) CH_4 and (d) N_2 at 273 K.

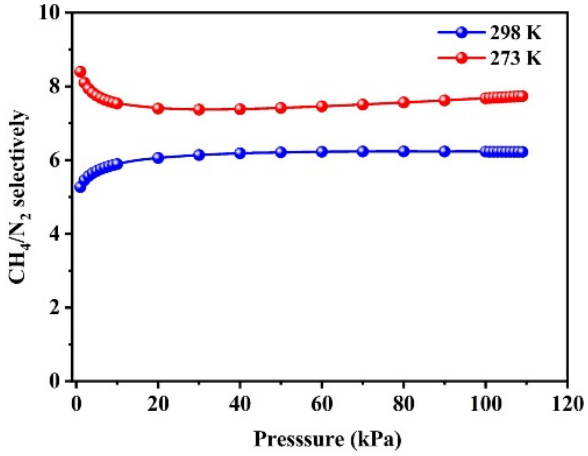

Figure S19. The IAST selectivity of $Zn_2(atz)_2ipa$-(*kg*) toward CH_4 over N_2 with altered pressures.

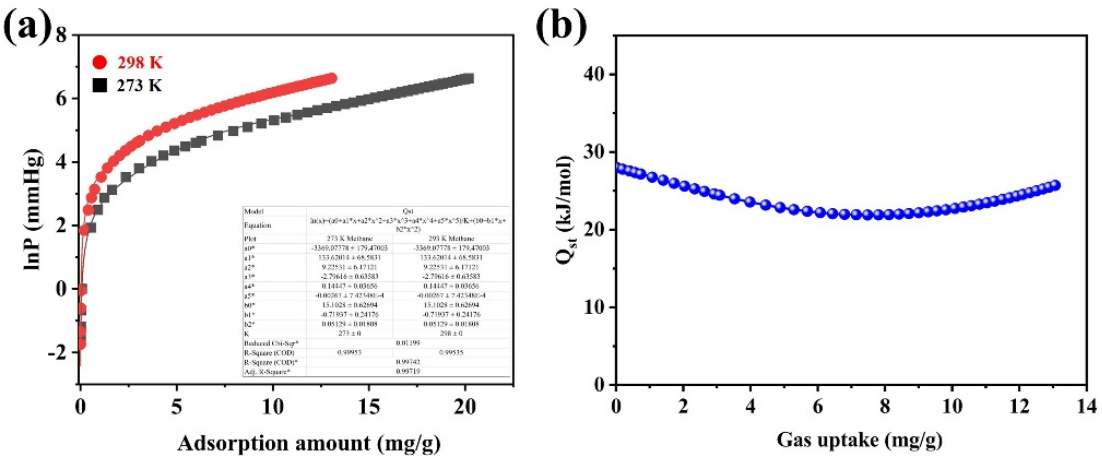

Figure S20. (a) Virial fitting of CH_4 adsorption isotherms for Q_{st} calculation. (b) The heat of CH_4 adsorption on $Zn_2(atz)_2ipa$-(*kg*) at different loadings.

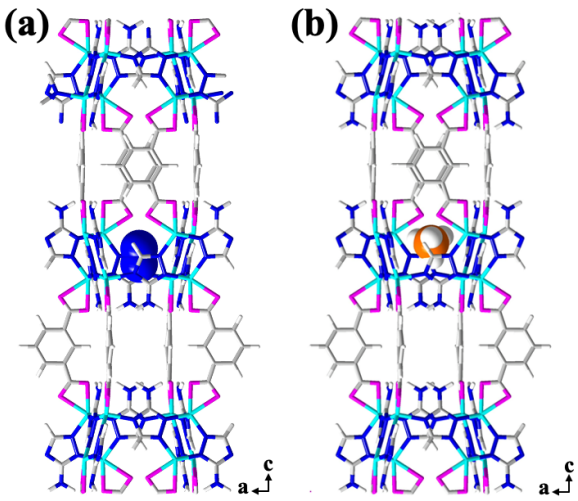

Figure S21. Preferred binding sites of (a) N_2 and (b) CH_4 on $Zn_2(atz)_2ipa$ calculated by DFT simulation.

References

1 K.-J. Chen, R.-B. Lin, P.-Q. Liao, C.-T. He, J.-B. Lin, W. Xue, Y.-B. Zhang, J.-P. Zhang and X.-M. Chen, *Cryst. Growth Des.*, 2013, **13**, 2118-2123.

2 P.-D. Zhang, J.-H. Liu, X.-Q. Wu, Y. Xie, J. Yu and J.-R. Li, *Sep. Purif. Technol.*, 2024, **333**, 125791.

3 J. VandeVondele, M. Krack, F. Mohamed, M. Parrinello, T. Chassaing and J. Hutter, *Comput. Phys. Commun.*, 2005, **167**, 103-128.

4 S. Goedecker, M. Teter and J. Hutter, *Phys. Rev. B*, 1996, **54**, 1703-1710.

5 C. Hartwigsen, S. Goedecker and J. Hutter, *Phys. Rev. B*, 1998, **58**, 3641-3662.

6 M. Krack and M. Parrinello, *Phys. Chem. Chem. Phys.*, 2000, **2**, 2105-2112.

7 J. VandeVondele and J. Hutter, *J. Chem. Phys.*, 2007, **127**, 114105.

8 J. P. Perdew, K. Burke and M. Ernzerhof, *Phys. Rev. Lett.*, 1996, **77**, 3865.

9 S. Grimme, J. Antony, S. Ehrlich and H. Krieg, *J. Chem. Phys.*, 2010, **132**, 154104.

10 S.-M. Wang, M. Shivanna and Q.-Y. Yang, *Angew. Chem. Int. Ed.* 2022, **61**, e202201017.

11 M. Chang, Y. Zhao, D. Liu, J. Yang, J. Li and C. Zhong, *Sustain. Energ. Fuels*, 2020, **4**, 138-142.

12 L. Li, L. Yang, J. Wang, Z. Zhang, Q. Yang, Y. Yang, Q. Ren and Z. Bao, *AlChE J.*, 2018, **64**, 3681-3689.

13 D. Lv, Y. Wu, J. Chen, Y. Tu, Y. Yuan, H. Wu, Y. Chen, B. Liu, H. Xi, Z. Li and Q. Xia, *AlChE J.*, 2020, **66**, e16287.

14 P. Guo, Y. Ying and D. Liu, *ACS Appl. Mater. Interfaces*, 2024, **16**, 7338-7344.

15 M. Chang, J. Ren, Q. Yang and D. Liu, *Chem. Eng. J.*, 2021, **408**, 127294.

16 Z. Niu, X. Cui, T. Pham, P. C. Lan, H. Xing, K. A. Forrest, L. Wojtas, B. Space and S. Ma, *Angew. Chem. Int. Ed.*, 2019, **58**, 10138-10141.

17 M. Chang, F. Wang, Y. Wei, Q. Yang, J.-X. Wang, D. Liu and J.-F. Chen, *AlChE J.*, 2022, **68**, e17794.

18 M. Chang, T. Yan, Y. Wei, J.-X. Wang, D. Liu and J.-F. Chen, *ACS Appl. Mater. Interfaces*, 2022, **14**, 25374-25384.

19 P. T. K. Nguyen, H. T. D. Nguyen, H. Q. Pham, J. Kim, K. E. Cordova and H. Furukawa, *Inorg. Chem.*, 2015, **54**, 10065-10072.

20 J. Hu, T. Sun, X. Liu, Y. Guo and S. Wang, *RSC Adv.*, 2016, **6**, 64039-64046.

21 Q. Shi, J. Wang, H. Shang, H. Bai, Y. Zhao, J. Yang, J. Dong and J. Li, *Sep. Purif. Technol.*, 2020, **230**, 115850.

22 S. Qadir, Y. Gu, S. Ali, D. Li, S. Zhao, S. Wang, H. Xu and S. Wang, *Chem. Eng. J.*, 2022, **428**, 131136.

23 X.-W. Liu, Y.-M. Gu, T.-J. Sun, Y. Guo, X.-L. Wei, S.-S. Zhao and S.-D. Wang, *Ind. Eng. Chem. Res.*, 2019, **58**, 20392-20400.

24 T. Li, X. Jia, H. Chen, Z. Chang, L. Li, Y. Wang and J. Li, *ACS Appl. Mater. Interfaces*, 2022, **14**, 15830-15839.

25 Z. Huang, P. Hu, J. Liu, F. Shen, Y. Zhang, K. Chai, Y. Ying, C. Kang, Z. Zhang and H. Ji, *Sep. Purif. Technol.*, 2022, **286**, 120446.

26 F. Zhang, Y. Tang, Z. Zhao, M. Lu, X. Wang, J. Li and J. Yang, *Inorg. Chem. Front.*, 2024, **11**,3889-3896.

27 C. E. Kivi, B. S. Gelfand, H. Dureckova, H. T. K. Ho, C. Ma, G. K. H. Shimizu, T. K. Woo and D. Song, *Chem. Commun.*, 2018, **54**, 14104-14107.

28 X. Wu, B. Yuan, Z. Bao and S. Deng, *J. Colloid Interf. Sci.*, 2014, **430**, 78-84.

29 J. Liu, X. Tang, X. Liang, L. Wu, F. Zhang, Q. Shi, J. Yang, J. Dong and J. Li, *AlChE J.*, 2022, **68**,

e17589.
30 Y. Guo, J. Hu, X. Liu, T. Sun, S. Zhao and S. Wang, *Chem. Eng. J.*, 2017, **327**, 564-572.
31 F. Zhang, H. Shang, B. Zhai, X. Li, Y. Zhang, X. Wang, J. Li and J. Yang, *AlChE J.*, 2023, **69**, e18079.
32 J. Hu, T. Sun, X. Liu, S. Zhao and S. Wang, *Micropor. Mesopor. Mater.*, 2016, **225**, 456-464.
33 T.-H. Kim, S.-Y. Kim, T.-U. Yoon, M.-B. Kim, W. Park, H. H. Han, C.-i. Kong, C.-Y. Park, J.-H. Kim and Y.-S. Bae, *Chem. Eng. J.*, 2020, **399**, 125717.
34 Y. He, S. Xiang, Z. Zhang, S. Xiong, F. R. Fronczek, R. Krishna, M. O'Keeffe and B. Chen, *Chem. Commun.*, 2012, **48**, 10856-10858.
35 X. Wang, L. Li, J. Yang and J. Li, *Chin. J. Chem. Eng.*, 2016, **24**, 1687-1694.
36 H. Ma, H. Ren, X. Zou, S. Meng, F. Sun and G. Zhu, *Polym. Chem.*, 2014, **5**, 144-152.
37 J. Möllmer, M. Lange, A. Möller, C. Patzschke, K. Stein, D. Lässig, J. Lincke, R. Gläser, H. Krautscheid and R. Staudt, *J. Mater. Chem.*, 2012, **22**, 10274-10286.
38 D. Saha, Z. Bao, F. Jia and S. Deng, *Environ. Sci. Technol.*, 2010, **44**, 1820-1826.
39 Q. Min Wang, D. Shen, M. Bülow, M. Ling Lau, S. Deng, F. R. Fitch, N. O. Lemcoff and J. Semanscin, *Micropor. Mesopor. Mater.*, 2002, **55**, 217-230.
40 B. Liu and B. Smit, *J. Phys. Chem. C*, 2010, **114**, 8515-8522.
41 L. Li, J. Yang, J. Li, Y. Chen and J. Li, *Micropor. Mesopor. Mater.*, 2014, **198**, 236-246.
42 J. Pérez-Pellitero, H. Amrouche, F. R. Siperstein, G. Pirngruber, C. Nieto-Draghi, G. Chaplais, A. Simon-Masseron, D. Bazer-Bachi, D. Peralta and N. Bats, *Chem.– Eur. J.*, 2010, **16**, 1560-1571.
43 Y. Zhang, W. Su, Y. Sun, J. Liu, X. Liu and X. Wang, *J. Chem. Eng. Data*, 2015, **60**, 2951-2957.
44 M. E. Rivera-Ramos and A. J. Hernández-Maldonado, *Ind. Eng. Chem. Res.*, 2007, **46**, 4991-5002.
45 M. Mofarahi and A. Bakhtyari, *J. Chem. Eng. Data*, 2015, **60**, 683-696.